External pH modulates EAG superfamily K^+ channels through EAG-specific acidic residues in the voltage sensor

Marcin Kazmierczak,[1] Xiaofei Zhang,[2] Bihan Chen,[2] Daniel K. Mulkey,[3] Yingtang Shi,[3] Paul G. Wagner,[3] Kendra Pivaroff-Ward,[2] Jessica K. Sassic,[1] Douglas A. Bayliss,[3] and Timothy Jegla[1]

[1]Department of Biology, The Pennsylvania State University, University Park, PA 16802
[2]Department of Cell Biology, The Scripps Research Institute, La Jolla, CA 92037
[3]Department of Pharmacology, University of Virginia, Charlottesville, VA 22908

The Ether-a-go-go (EAG) superfamily of voltage-gated K^+ channels consists of three functionally distinct gene families (Eag, Elk, and Erg) encoding a diverse set of low-threshold K^+ currents that regulate excitability in neurons and muscle. Previous studies indicate that external acidification inhibits activation of three EAG superfamily K^+ channels, Kv10.1 (Eag1), Kv11.1 (Erg1), and Kv12.1 (Elk1). We show here that Kv10.2, Kv12.2, and Kv12.3 are similarly inhibited by external protons, suggesting that high sensitivity to physiological pH changes is a general property of EAG superfamily channels. External acidification depolarizes the conductance–voltage (GV) curves of these channels, reducing low threshold activation. We explored the mechanism of this high pH sensitivity in Kv12.1, Kv10.2, and Kv11.1. We first examined the role of acidic voltage sensor residues that mediate divalent cation block of voltage activation in EAG superfamily channels because protons reduce the sensitivity of Kv12.1 to Zn^{2+}. Low pH similarly reduces Mg^{2+} sensitivity of Kv10.1, and we found that the pH sensitivity of Kv11.1 was greatly attenuated at 1 mM Ca^{2+}. Individual neutralizations of a pair of EAG-specific acidic residues that have previously been implicated in divalent block of diverse EAG superfamily channels greatly reduced the pH response in Kv12.1, Kv10.2, and Kv11.1. Our results therefore suggest a common mechanism for pH-sensitive voltage activation in EAG superfamily channels. The EAG-specific acidic residues may form the proton-binding site or alternatively are required to hold the voltage sensor in a pH-sensitive conformation. The high pH sensitivity of EAG superfamily channels suggests that they could contribute to pH-sensitive K^+ currents observed in vivo.

The Journal of General Physiology

INTRODUCTION

Ether-a-go-go (EAG) superfamily voltage-gated K^+ channels have the characteristic property of a low activation threshold, suggesting that they are well-adapted to control the intrinsic excitability of neurons. Indeed, the founding member of the gene superfamily, *Drosophila melanogaster eag*, was cloned on the basis of a hyperexcitable phenotype in which flies shook under ether anesthesia (Ganetzky and Wu, 1983). The superfamily comprises three evolutionarily conserved gene families, Eag (Kv10), Erg (Kv11), and Elk (Kv12), defined by sequence homology and functional independence; heterotetramers can form within but not across the gene families (Wimmers et al., 2001; Schönherr et al., 2002; Zou et al., 2003), indicating that each family encodes a nonoverlapping set of functional channels. Despite the fact that the eight mammalian members of the EAG superfamily are widely expressed throughout the nervous system, we are only beginning to learn about their physiological roles. The mouse Elk K^+ channel Kv12.2 contributes to subthreshold K^+ currents in hippocampal neurons. Genetic deletion lowers the action potential threshold in these neurons, causing seizures (Zhang et al., 2010). The Erg family member Kv11.1 (hErg1) is known to play a crucial role in regulating the length of heart action potential repolarization (Sanguinetti and Tristani-Firouzi, 2006), and in the brain, Erg channels were recently implicated in regulating the excitability in mouse auditory brainstem (Hardman and Forsythe, 2009) and limiting the rate of spontaneous firing of midbrain dopaminergic neurons (Ji et al., 2012). The phenotype of the Eag *Drosophila* orthologue mutant has been characterized (Wu et al., 1983; Srinivasan et al., 2012), and mouse Kv10.1 deletion results only in modest hyperactivity (Ufartes et al., 2013). Ectopic expression of Kv10.1 in mammals has been observed in diverse types of tumors (Hemmerlein et al., 2006; Agarwal et al., 2010).

Correspondence to Timothy Jegla: tjj3@psu.edu
D.K. Mulkey's present address is Dept. of Physiology and Neurobiology, University of Connecticut, Storrs, CT 06269.
P.G. Wagner's present address is Biology Dept., Washburn University, Topeka, KS 66621.

Abbreviations used in this paper: EAG, Ether-a-go-go; TEVC, two-electrode voltage clamp.

The Rockefeller University Press $30.00
J. Gen. Physiol. Vol. 141 No. 6 721–735
www.jgp.org/cgi/doi/10.1085/jgp.201210938

One overlooked characteristic of the EAG superfamily that could have significance in vivo is their sensitivity to physiological changes in extracellular pH. One member of each gene family, Kv10.1 (Eag1; Terlau et al., 1996), Kv11.1 (Erg1; Anumonwo et al., 1999; Bérubé et al., 1999; Jo et al., 1999; Terai et al., 2000), and Kv12.1 (Elk1; Shi et al., 1998), has been reported to be inhibited by extracellular acidosis. The neurophysiology of acid-sensitive TASK channels has been highly studied (Duprat et al., 1997; Reyes et al., 1998; Rajan et al., 2000; Berg et al., 2004; Lin et al., 2004; Cho et al., 2005; Putzke et al., 2007), but genetic evidence now makes it clear that they do not account for all pH-sensitive K^+ currents observed in vivo. For example, acid-inhibited K^+ currents that regulate firing rate in the intrinsically chemosensitive respiratory neurons of the retrotrapezoid nucleus (Mulkey et al., 2004) and glucose-sensing orexin-positive hypothalamic neurons (Yamanaka et al., 2003) are intact in the TASK1-TASK3 double-knockout mice (Mulkey et al., 2007; González et al., 2009; Guyon et al., 2009). Although TASK2 channels are expressed in CO_2/pH-responsive retrotrapezoid nucleus respiratory neurons, respiratory chemosensitivity is retained in TASK2 knockout mice, suggesting that TASK2 is not the main pH-sensitive potassium channel in those cells (Gestreau et al., 2010). Although no genetic evidence has yet been produced to directly show that EAG superfamily channels underlie pH-sensitive K^+ currents in vivo, their subthreshold activation and strong pH sensitivity make them excellent candidates for pH-sensitive currents that cannot be explained by TASK channels. Therefore, we explored whether pH sensitivity might be a general attribute of EAG superfamily channels and examined the molecular mechanism.

Acid inhibition of TASK channels, which do not contain a voltage sensor, occurs primarily through protonation of a histidine residue adjacent to the selectivity filter; protonation directly reduces TASK channel opening (Kim et al., 2000; Rajan et al., 2000). In contrast, a major effect of extracellular acidosis in the EAG superfamily channels Kv10.1, Kv12.1, and Kv11.1 is to shift conductance–voltage (GV) relations toward more depolarized potentials (Terlau et al., 1996; Shi et al., 1998; Jiang et al., 1999). Slowing of activation gating by external protons was reported for Kv10.1 (Terlau et al., 1996) and Kv11.1 (Zhou and Bett, 2010) but not Kv12.1 (Shi et al., 1998). Extracellular pH also accelerates Kv11.1 deactivation (Anumonwo et al., 1999; Jiang et al., 1999) and decreases its open channel conductance via proton pore block (Van Slyke et al., 2012).

The ability of extracellular protons to alter voltage-dependent gating in EAG superfamily channels raises the possibility that the voltage sensor is a direct target for protonation. Further support for this hypothesis comes from experiments showing that protons reduce the ability of Mg^{2+} to slow voltage-dependent activation of Kv10.1, suggesting a possible overlap in binding sites (Terlau et al., 1996). The Mg^{2+}-binding site of Eag family channels lies in an external aqueous pocket in the voltage sensor (Silverman et al., 2000). Because Mg^{2+} impedes early gating transitions that occur independently in each voltage sensor of the tetrameric channel (Terlau et al., 1996; Tang et al., 2000), it seems unlikely that binding of protons outside the voltage sensor would allosterically reduce Mg^{2+} sensitivity.

A similar divalent binding site is conserved in Elk and Erg family channels (Silverman et al., 2000; Fernandez et al., 2005; Zhang et al., 2009; Abbruzzese et al., 2010), providing a possible explanation for inhibition of voltage-dependent activation by protons in Kv11.1 and Kv12.1. The divalent binding sites of the subfamilies differ substantially in selectivity. For instance, Mg^{2+} and Ni^{2+} potently block Eag channels (Terlau et al., 1996; Silverman et al., 2004) but have little effect on the Elk channel Kv12.1, which is preferentially blocked by Zn^{2+} (Zhang et al., 2009). Ca^{2+} inhibits Kv11.1 and lowers its pH sensitivity (Jo et al., 1999). Despite these differences in selectivity, the EAG superfamily divalent binding site is highly conserved and has the potential for pH titration: it primarily consists of three solvent-accessible acidic residues in the S2 and S3 transmembrane domains that are conserved across the EAG superfamily (Silverman et al., 2000; Fernandez et al., 2005; Zhang et al., 2009; Abbruzzese et al., 2010). Schematic drawings of the EAG voltage sensor with six acidic residue positions marked and divalent binding site are presented in Fig. 1 (A and B). Acidic residues at positions 1, 5, and 6 in transmembrane domains S2 and S3 are solvent exposed from the extracellular side and form the core of the divalent binding site. Sequence alignments of EAG superfamily channels with HCN1, CNG2A, and Shaker are shown for S2, S3, and S4 in Fig. 1 C. Acidic position 1 in S2 is conserved as an acidic side chain in most voltage-gated ion channel families and will be referred to here as the universal acidic residue. The acidic residues at positions 5 and 6 in S2 and S3 will be referred to here as the EAG-specific acidic residues because they are unique to the EAG superfamily among K^+ channels. However, these acidic residues are also present in cyclic nucleotide–gated and hyperpolarization-gated cation channels; EAG K^+ channels share a closer evolutionary relationship with these cation channels than with other voltage-gated K^+ channels (Yu and Catterall, 2004). Residues at the outer edge of S4 also contribute to Mg^{2+} block in Kv10.2, Zn^{2+} block in Kv12.1, and Ca^{2+} block in Kv11.1 (Johnson et al., 2001; Zhang et al., 2009) but are not highly conserved across subfamilies.

The purpose of this study was to examine the hypothesis that extracellular protons inhibit voltage activation of EAG superfamily channels by protonation of acidic residues that comprise the divalent binding site. This hypothesis predicts that proton-dependent inhibition

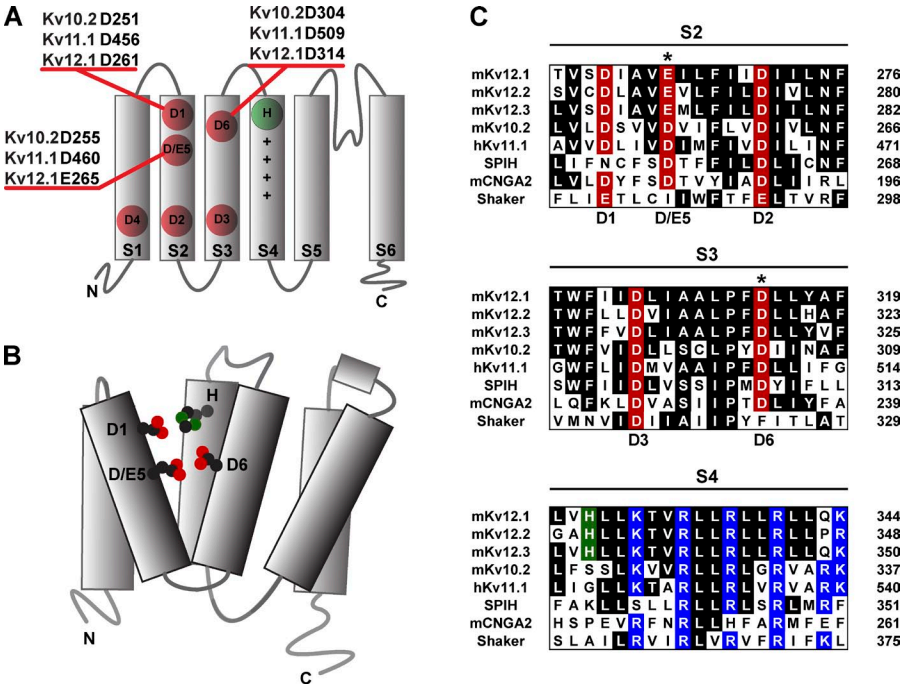

Figure 1. Acidic residues in the voltage sensor of EAG superfamily channels. (A) A single subunit of a tetrameric EAG superfamily K^+ channel is diagrammed with transmembrane domains S1–S6 depicted as rectangles. S1–S4 form the voltage sensor, and S5–S6 constitute the conduction pathway. Acidic residues of the voltage sensor are marked in red. Basic gating charges in the S4 helix are depicted with + symbols, and an Elk-specific histidine residue at the outer edge of S4 is marked in green. Acidic residues 1–3 are highly conserved across voltage-gated cation channels, and acidic residues 4–6 are specific to the EAG superfamily (among K^+ channels). Residue positions for the three S2/S3 acidics that are accessible from the extracellular side (D1, D/E5, and D6) are given for mouse Kv10.2, human Kv11.1, and mouse Kv12.1. (B) Schematic structural drawing of a single subunit of an Elk family K^+ channel. Side chains of four residues participating in binding of divalent cations are depicted with oxygens and nitrogens highlighted in red and green, respectively. These residues (D1, E5, D6, and the Elk-specific histidine in S4) are predicted to lie in close proximity within an aqueous cleft in the outer voltage sensor. (C) Amino acid alignments of the transmembrane voltage sensor helices S2–S4 are shown for various EAG superfamily K^+ channels, the olfactory CNG channel α subunit (CNGA2), a sea urchin HCN channel (SPIH), and *Drosophila* Shaker. Species prefixes m and h in the channel names refer to mouse and human, respectively. Conserved residues are shaded. Acidic residues are labeled in red and marked with the position numbers defined in A. Asterisks mark the EAG-specific acidic residue positions in S2 and S3. Basic residues and Elk-specific histidine in S4 are highlighted in blue and green, respectively.

of voltage activation should be a general feature of EAG superfamily channels and that neutralization of one or more acidic divalent binding residues should reduce pH sensitivity. Here we present evidence that extracellular acidification inhibits voltage activation of three additional EAG family channels (Kv10.2, Kv12.2, and Kv12.3). Furthermore, we show that the EAG-specific acidic residues of the divalent binding site are required for high pH sensitivity in Elk (Kv12.1), Eag (Kv10.2), and Erg (Kv11.1) channels.

MATERIALS AND METHODS

Expression in *Xenopus laevis* oocytes

Mouse Kv12.1, Kv12.2, and Kv10.2 and human Kv11.1 cDNAs were cloned from cDNA libraries using PCR, sequence verified, and transferred into the pOX plasmid (Jegla and Salkoff, 1997) for expression in *Xenopus* oocytes. Mutations were introduced using standard PCR-based mutagenesis, and all constructs were sequence-confirmed. Capped run-off cRNA transcripts were generated from linearized expression plasmids using T3 mMessage mMachine and Poly-A tailing kits (Life Technologies). Samples were cleaned by LiCl precipitation and diluted in nuclease-free water supplemented with RNASE inhibitor (SUPERase-In; Life Technologies) before use. *Xenopus* oocytes were purchased from Nasco and enzymatically defolliculated with 1 mg/ml type II collagenase. Mature oocytes were injected with 1–5 ng cRNA in a 50-nl volume and incubated 1–3 d before recording at 18°C in ND96 (96 mM NaCl, 2 mM KCl, 2 mM $CaCl_2$, 1 mM $MgCl_2$, and 5 mM HEPES, pH 7.2) supplemented with 2.5 mM Na-pyruvate, 100 U/ml penicillin, and 100 µg/ml streptomycin. $CaCl_2$, Na-pyruvate, penicillin, and streptomycin were removed for collagenase digestion. Chemical reagents were purchased from Sigma-Aldrich, unless otherwise noted.

Xenopus oocyte recordings

Recordings were performed using a CA-1B amplifier (Dagan) in two-electrode voltage clamp (TEVC) mode at room temperature (22–24°C). Microelectrodes (<1 MΩ) were filled with 3 M KCl, and bath clamp circuitry was connected by a 1 M NaCl/agarose bridge. Base recording solution used for Kv12.1, Kv12.2, and Kv11.1 consisted of (in mM) 98 NaOH, 2 KCl, 1 CaCl, and 5 HEPES and was adjusted to the desired pH value with methanesulfonic acid. Methanesulfonate was therefore the major solution anion. 1 mM Mg^{2+} was used in some recordings of Kv12.1 and Kv12.2, and Ca^{2+} concentration was adjusted as indicated for Kv11.1. These channels are less sensitive to Mg^{2+} and it had little effect on their pH sensitivity. We removed Mg^{2+} for later experiments because of its ability to inhibit activation and reduce pH sensitivity of Kv10.2. For Kv10.2 recordings, K^+ concentration was increased to 50 mM by substituting NaOH with KOH to allow recording of tail currents at −100 mV where Cole-Moore shifts did not significantly affect tail current magnitude.

Data collection and analysis were performed using pCLAMP acquisition suite (Molecular Devices). GV curves were measured from isochronal tail currents recorded at −100 mV for Kv10.2 or −40 mV for Kv12.1, Kv12.2, and Kv11.1. Data were fit in Origin 8.1 (OriginLab) with a single Boltzmann distribution: $f(V) = (A_1 - A_2)/(1 + e^{(V-V_{50})/s}) + A_2$, where V_{50} is the half-maximal activation point, s is the slope factor, and A_1 and A_2 are the asymptotes, respectively. Reported V_{50} and slope factor values show the

mean ± SEM of individual fits. Data from individual cells were normalized before averaging for display; they are plotted with a single Boltzmann distribution: $G/G_{MAX} = 1/(1+e^{-(V-\hat{V}_{50})/\hat{s}})$, where $\hat{V}_{50}$ and $\hat{s}$ are the arithmetic means of half-maximal activation potentials and slope factors, respectively. The pK_a of Kv12.1 and Kv12.2 was estimated by fitting a simple three-parameter dose–response curve to V_{50} values obtained at various pH values: $V_{50}(pH) = A_1 + (A_2 - A_1)/(1+10^{pH-pK_a})$, where A_1 and A_2 determine the asymptotes and pK_a is the value of pH for the half-maximal shift of V_{50}. A four-parameter dose–response curve was used to fit pH-dependent V_{50} shifts at various Ca^{2+} concentrations for Kv11.1: $\Delta V_{50}([Ca^{2+}]) = A_1 + (A_2 - A_1)/(1+10^{h(pH-pK_a)})$. Activation rate was estimated by measuring the time at which currents achieved 80% of their maximal value during a test depolarization (t_{80}). Two-sample two-tailed nonequal variance Student's *t* tests were used to assess statistical significance and p-values.

Expression and recordings in HEK293 cells

Human Elk channels hKv12.1, hKv12.2, and hKv12.3 were transfected into HEK293 cells together with GFP (pEGFP) by using Lipofectamine 2000 (Life Technologies). Whole cell patch clamp recordings were obtained from GFP-labeled cells at room temperature using 3–5-MΩ patch pipettes and an Axopatch 200B amplifier (Molecular Devices). Bath solution was composed of (in mM) 140 NaCl, 3 KCl, 2 $MgCl_2$, 2 $CaCl_2$, 10 HEPES, and 10 glucose; pH was adjusted to levels indicated using HCl or NaOH. Internal solution contained (in mM) 120 KMES, 4 $NaCl_2$, 1 $MgCl_2$, 0.5 $CaCl_2$, 10 HEPES, 10 EGTA, 3 Mg-ATP, and 0.3 GTP-Tris, pH 7.2. Holding current at −60 mV was obtained at 5-s intervals during constant perfusion using the pCLAMP acquisition package (Molecular Devices). The dependence of holding current on pH was normalized, and a fixed end-point fit of a four-parameter dose–response curve was applied.

Online supplemental material

Fig. S1 presents GV curves at pH 6, 7, and 8 for additional Kv12.1 H328 mutants (H328Q, H328K, H328Y, and H328E) and analysis of the pH sensitivity of activation kinetics for Kv12.1 H328A and H328R; mutants were sequence-confirmed, and currents were recorded from *Xenopus* oocytes by TEVC. Online supplemental material is available at http://www.jgp.org/cgi/content/full/jgp.201210938/DC1.

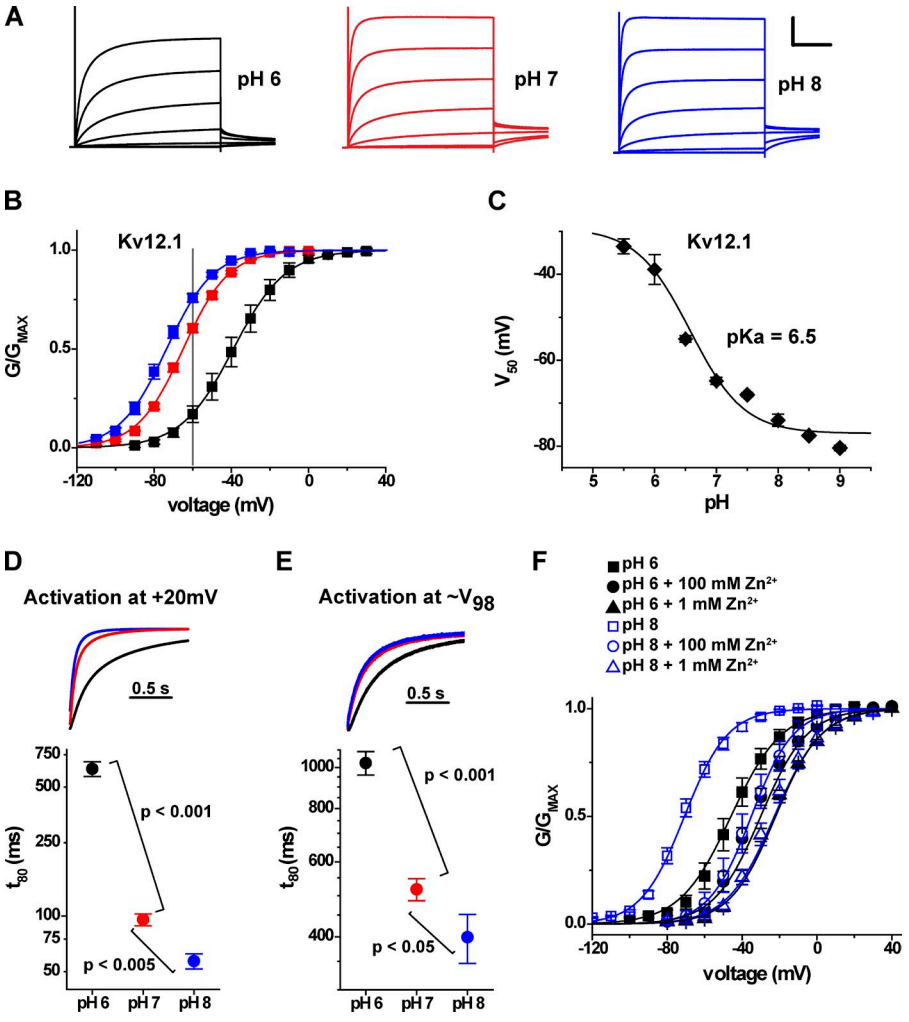

Figure 2. Effect of extracellular pH on voltage activation of Kv12.1. (A) Kv12.1 current traces elicited by 4-s depolarization steps from −100 to 20 mV (in 20-mV increments from a holding potential of −100 mV) are shown for bath solutions of pH 6, 7, and 8. Tail step voltage was −40 mV. Recordings were made from a single *Xenopus* oocyte using TEVC. Scale bar: 2.5 µA, 1 s. (B) Normalized GV relations for Kv12.1 at pH 6 (black), 7 (red), and 8 (blue). Conductance values were taken from isochronal tail currents recorded at −40 mV after 4-s depolarization steps to the indicated voltages. Error bars show SEM (n = 3–8), and lines show single Boltzmann distribution fits. The gray line at −60 mV indicates the voltage used in Fig. 4 to examine pH-dependent changes in holding current for Kv12.1. (C) Plot of V_{50} versus pH for Kv12.1. V_{50} values were determined as in B, and the curve shows a three-parameter dose–response fit yielding a pK_a value of 6.5. Error bars show SEM (n = 3–8). (D) Current traces from the 20-mV voltage step in A are normalized and superimposed to highlight changes of activation time course; bath pH is encoded by color as in A. The graph shows the time necessary for Kv12.1 to reach 80% activation (t_{80}) during steps to 20 mV (from a holding potential of −100 mV) at pH 6, 7, and 8. A $\log_{10}$ scale was applied to the t_{80} axis to better visualize the entire range of values, and statistical significance was judged using a two-tailed nonequal variance Student's *t* test. (E) Data are analyzed and presented as in D, but normalized for V_{50} shift: the voltages selected for each pH were −30 mV for pH 8, −20 mV for pH 7, and 10 mV for pH 6 and corresponded as closely as possible to the same open probability, ~V_{98}. Data in D and E are mean ± SEM (n = 8). (F) Comparison of Zn^{2+}-dependent shifts in Kv12.1 GV relationships at pH 6 and 8; data (mean ± SEM; n = 3–5) are shown for controls (squares), 100 µM Zn^{2+}, and 1 mM Zn^{2+}, and curves show single Boltzmann distribution fits.

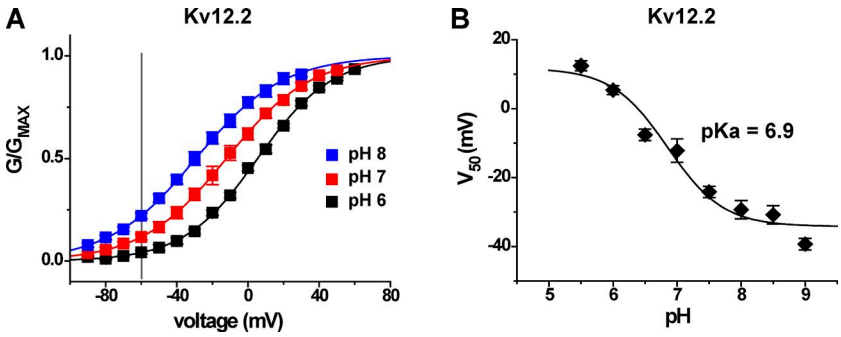

Figure 3. Effect of extracellular pH on voltage activation of Kv12.2. (A) Normalized GV curves determined in bath solutions of pH 6, 7, and 8 for Kv12.2; experiments were performed as described for Fig. 2 B, except depolarizing steps were limited to 2 s. Data points are mean, error bars show SEM (n = 3–5), curves depict single Boltzmann distribution fits, and the gray line marks −60 mV. (B) V_{50} versus pH is plotted for Kv12.2 with a three-parameter dose–response fit (pK_a 6.9).

RESULTS

Extracellular acidification inhibits voltage-dependent activation of mammalian Elk channels

We first characterized the response of the mouse Elk channel Kv12.1 to external pH changes in further detail to determine whether proton block resembles divalent block. The voltage activation range of rat Kv12.1 (Elk1) is depolarized by extracellular acidification (Shi et al., 1998). Mouse Kv12.1 K^+ currents recorded in response to 4-s depolarizing voltage steps in pH 6, 7, and 8 are shown in Fig. 2 A. Acidification depolarized the GV curve from a V_{50} of −74 ± 1 mV (n = 4) at pH 8 to a V_{50} of −39 ± 3 mV (n = 4) at pH 6 (Fig. 2 B). A dose–response fit of V_{50} values versus pH yields a pK_a of 6.5, indicating significant sensitivity in the physiological range (Fig. 2 C). External acidification also significantly slowed the activation time course of Kv12.1 currents

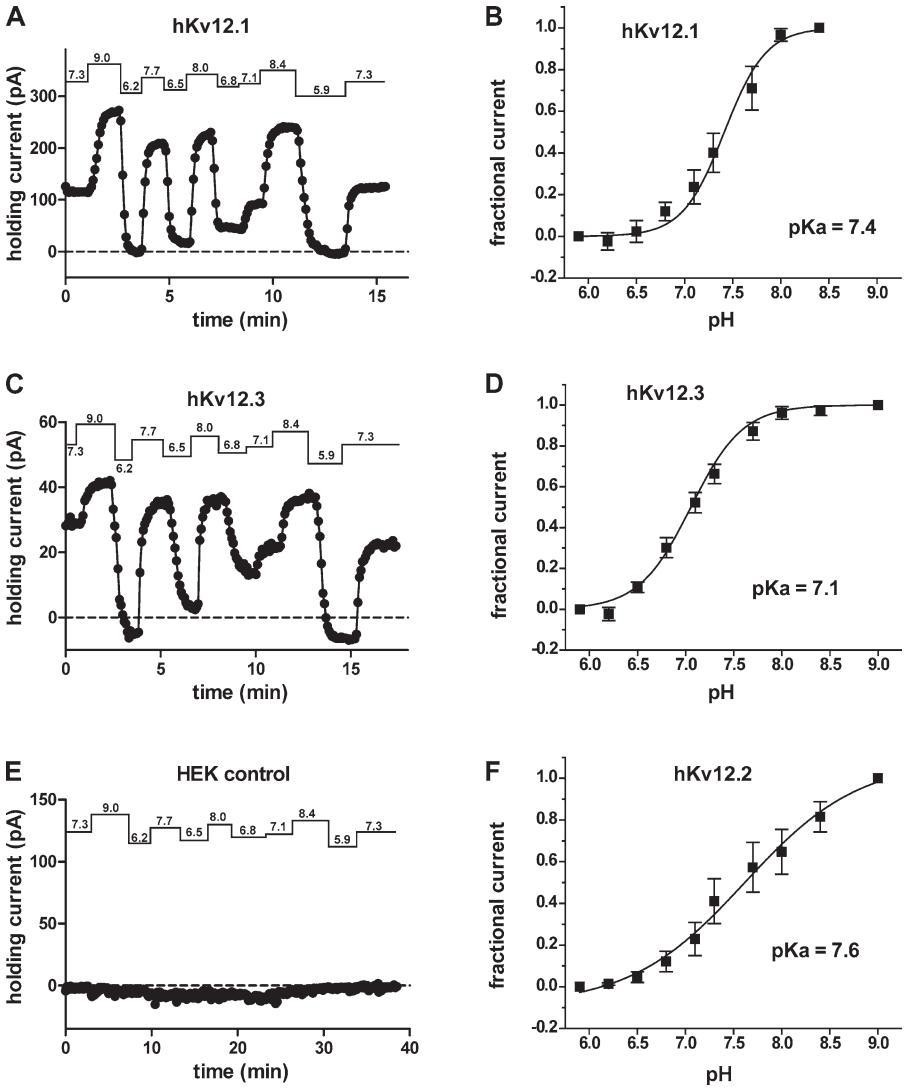

Figure 4. Effect of bath pH changes on holding current in HEK293 cells expressing Elk channels. (A and C) Holding current versus time plots are shown for whole cell patch recordings of HEK293 cells expressing human Kv12.1 channel (A) and Kv12.3 channel (C) during a series of bath pH changes (values indicated above). Data points were taken every 5 s. A typical recording from an untransfected control cell is shown in E. (B, D, and F) Plots of holding current versus pH are given for human Kv12.1 (B), Kv12.3 (D), and Kv12.2 (F) channels. Data from individual cells were normalized to the magnitude of the holding current obtained at the highest and lowest bath pH values examined. Data points show mean ± SEM (n = 4–6), and curves show a four parameter dose–response fit with the predicted pK_a value indicated.

when measured at a constant voltage (Fig. 2 D). A move from pH 8 to 6 increased the time to reach 80% activation during a 20-mV step ~10-fold from 57 ± 5 ms (n = 6) to 629 ± 58 ms (n = 8). Some of the slowing was accounted for by the shift in GV, but activation remained significantly slower at low pH when we compared the activation time course at equivalent points on the GV curve (~V_{98}; Fig. 2 E). The effects of protons on activation time course and V_{50} are qualitatively similar to the effects of Zn^{2+}, which binds at the EAG superfamily divalent binding site in the outer voltage sensor (Zhang et al., 2009).

We next investigated the pH sensitivity of Zn^{2+}-dependent inhibition of activation in Kv12.1 to test whether proton inhibition might share a common mechanism with divalent block. Fig. 2 F shows the sensitivity of Kv12.1 to Zn^{2+} at pH 8 and 6. We used 8-s voltage steps in these experiments because of extremely slow activation in the presence of Zn^{2+}. The V_{50} shift caused by 1 mM Zn^{2+} was significantly reduced from 46 ± 2 mV in pH 8 to 20 ± 1 mV in pH 6 ($P < 0.0001$). This result is perfectly analogous to the reduction in Mg^{2+} block observed at low pH for Kv10.1 (Terlau et al., 1996) and suggests that protons may inhibit voltage-dependent activation of both channels by a similar mechanism. The competitive action of protons and divalents in these channels cannot be explained by a nonspecific effect of surface charge saturation because we did not observe inhibition of pH sensitivity for Kv12.1 in the presence of 1 mM Mg^{2+}, which selectively blocks Kv10 channels. Hence, our result suggests a possible overlap in binding sites for protons and Zn^{2+} within the Kv12.1 channel.

We reasoned that pH sensitivity could therefore be a general property of Elk family channels because the residues of the divalent binding site are highly conserved. We found that Kv12.2, a channel which regulates excitability in hippocampal pyramidal neurons (Zhang et al., 2010), has a very similar sensitivity to external pH, both in terms of magnitude of V_{50} shift and pK_a (Fig. 3, A and B). The V_{50} of Kv12.2 shifted from −29 ± 3 mV (n = 5) in pH 8 to 5 ± 1 mV (n = 4) in pH 6. A dose–response fit of V_{50} values versus pH for Kv12.2 channel gives a pK_a of 6.9. An apparent divergence between fits and the measured V_{50} values at high pH for both Kv12.1 and Kv12.2 suggests the possibility of an additional minor site for pH-dependent modulation of voltage gating with pK_a > 8. We focused the current research on the major effects observed between pH 6 and 8 and did not study this minor component further.

We next investigated the potential for physiological relevance of Elk channel pH sensitivity by examining the effect of bath pH changes on the holding current required to clamp HEK293 cells expressing various Elk channels to −60 mV, a value in the range of typical neuronal resting potentials. Because the pH-dependent changes of open probability at −60 mV are significant for both Kv12.1 and Kv12.2 (Figs. 2 B and 3 A, vertical lines indicate −60 mV), we expected an increase in outward holding current at high pH and decrease at low pH. Indeed, all members of the mammalian Elk family (Kv12.1, Kv12.2, and Kv12.3) showed the expected pH-dependent changes in holding current. Fig. 4 (A and C) shows examples of holding current variations recorded in response to bath pH changes in cells expressing Kv12.1 and Kv12.3, respectively. pH sensitivity has not previously been reported for Kv12.3. Normalized holding current versus pH for the three Kv12 channels is plotted against a four-parameter dose–response fit in Fig. 4 (B, D, and F) and follows the same predicted pattern of pH sensitivity in all channels. Fits yielded pK_a values

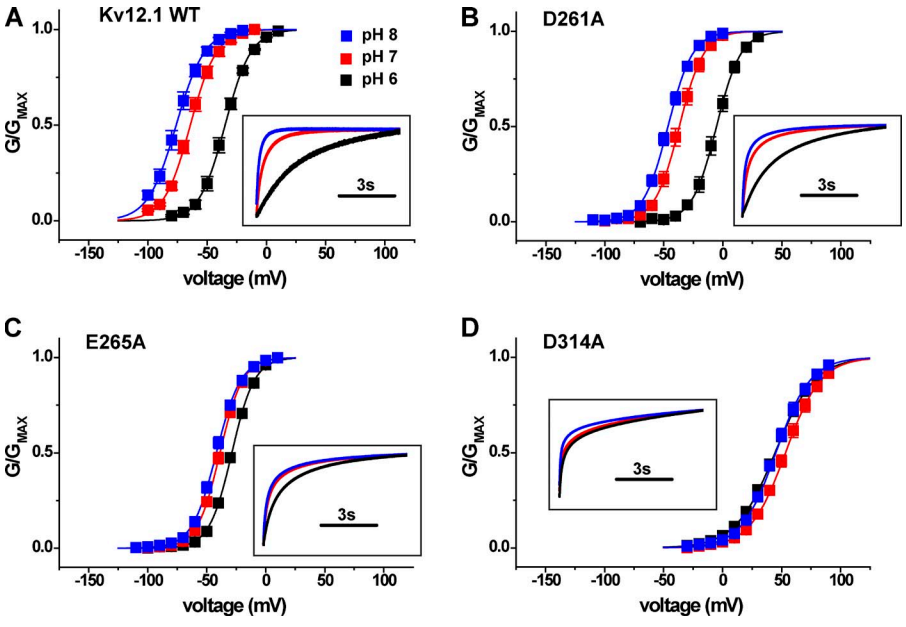

Figure 5. EAG superfamily–specific acidic residues in the voltage sensor are required for modulation of Kv12.1 activation by extracellular pH. (A–D) Normalized GV curves for WT Kv12.1, D261A (D1A), E265A (E5A), and D314A (D6A) are compared at bath pH values of 6, 7, and 8. Conductance was determined from isochronal tail currents recorded at −40 mV after 8-s steps to the indicated voltages; values show mean ± SEM (n = 4–8). Curves show single Boltzmann distribution fits. Fit parameters (V_{50} and slope factor) are reported in Table 1. Boxed insets show normalized and superimposed current traces for depolarization steps that correspond most closely to V_{95} asymptotic open probability at pH 7 for each mutant (−30 mV for WT, −10 mV for D261A, −10 mV for E265A, and 90 mV for D314A).

ranging from 7.1 in Kv12.3 to 7.6 in Kv12.2. These pK_a values are somewhat higher compared with those obtained from V_{50} measurements and most likely reflect differences in the method of measurement. Untransfected HEK293 cells did not show significant pH-dependent changes in holding current (Fig. 4 E). These results demonstrate that all mammalian Elk channels are highly sensitive to changes in extracellular pH, as expected if the conserved residues of the divalent binding site are involved in proton block.

EAG-specific acidic residues in the voltage sensor confer pH sensitivity to Kv12.1

We reasoned that the site for pH modulation in Kv12.1 could include the universal and/or EAG-specific acidic residues in S2 and S3 because these residues (a) contribute to divalent cation binding in Eag and Elk channels and (b) are conserved as acidic residues in all EAG superfamily channels. Although the pK_a values of individual glutamate and aspartate residues are not typically physiological, proximal acidic residues can have increased pK_a values reaching physiological range as the result of interaction (Harris and Turner, 2002). Structural models of the divalent binding site suggest close proximity of these acidic side chains within an aqueous pocket as schematically illustrated in Fig. 1 B (Silverman et al., 2004; Zhang et al., 2009). Neutralization of each of these three acidic charges with alanine reduces Zn^{2+} block in Kv12.1 (Zhang et al., 2009), so we examined the pH sensitivity of these mutants. Separate neutralization of the EAG-specific acidic charges E265A (E5) and D314A (D6), but not the universal charge D261A (D1), significantly reduced the pH sensitivity of Kv12.1 as measured by V_{50} shift between pH 8 and 6 (Fig. 5, A–D). Activation rate also appeared less sensitive to pH changes in these mutants (Fig. 5, A–D, insets),

TABLE 1

V_{50} and slope factor values from single Boltzmann fits of the GV relations

Channel	*n*	pH 6		pH 7		pH 8	
		V_{50}	*s*	V_{50}	*s*	V_{50}	*s*
		mV	*mV*	*mV*	*mV*	*mV*	*mV*
Kv12.2							
WT	4	5 ± 1	20.8 ± 0.5	−13 ± 3	23.4 ± 0.6	−29 ± 3	24 ± 1
Kv12.1							
WT[a]	6	−35 ± 2	11 ± 1	−65 ± 2	11 ± 1	−76 ± 2	12 ± 1
D261A	4	−5 ± 2	10 ± 1	−37 ± 2	10.3 ± 0.5	−46 ± 1	10.2 ± 0.4
D261E	6	−56 ± 2	12.3 ± 0.3	−109 ± 1	11.2 ± 0.5	−135 ± 2	10.2 ± 0.5
E265A	4	−28.7 ± 0.9	9.6 ± 0.4	−39 ± 1	9.6 ± 0.2	−42 ± 1	10.4 ± 0.2
E265D	7	−52 ± 1	11.3 ± 0.3	−72 ± 1	12.7 ± 0.8	−89 ± 2	13.2 ± 0.7
D314A	8	44 ± 2	16.8 ± 0.9	53 ± 2	15.1 ± 0.7	45 ± 2	14.6 ± 0.9
D314E	8	−70 ± 2	13 ± 1	−69 ± 2	14 ± 1	−64 ± 2	11.4 ± 0.9
H328A	8	−42 ± 3	13.9 ± 0.8	−62 ± 1	12.8 ± 0.6	−78 ± 0.5	12.6 ± 0.3
H328R	6	0 ± 1	16 ± 1	−4 ± 1	14.2 ± 0.6	−6 ± 1	14.4 ± 0.6
H328W	6	−18 ± 2	14.2 ± 0.8	−32 ± 3	15.4 ± 0.4	−37 ± 2	14.7 ± 0.5
H328R D261A	7	14 ± 1	12.0 ± 0.3	−11 ± 3	16.5 ± 0.9	−20 ± 3	17.8 ± 0.8
Kv10.2							
WT	11	−24 ± 2	22 ± 1	−71 ± 3	18.0 ± 0.3	−95 ± 3	15.8 ± 0.2
D251N	10	14 ± 2	21.5 ± 0.4	−32 ± 2	20.8 ± 0.4	−57 ± 3	21.9 ± 0.5
D255C	4	−9 ± 7	34 ± 2	−25 ± 8	38 ± 3	−31 ± 6	38 ± 3
D304N	8	−23 ± 2	18.0 ± 0.7	−35 ± 2	17.1 ± 0.5	−37 ± 2	17.5 ± 0.7
D304E	9	−1 ± 3	28 ± 1	−38 ± 2	20.1 ± 0.4	−75 ± 2	13.7 ± 0.3
Kv11.1							
WT	5	−16.4 ± 0.8	7.1 ± 0.3	−26.9 ± 0.5	7.7 ± 0.3	−28.8 ± 0.4	8.2 ± 0.5
D456C 1 mM Ca^{2+}	9	34 ± 2	13.1 ± 0.6	12 ± 1	13.5 ± 0.8	1 ± 1	15.9 ± 0.7
D460C 1 mM Ca^{2+}	9	24 ± 1	10.7 ± 0.4	10 ± 1	12.5 ± 0.4	4 ± 1	13.0 ± 0.7
D509C 1 mM Ca^{2+}	6	25 ± 2	12.6 ± 0.3	17 ± 2	12.9 ± 0.3	11 ± 1	13.7 ± 0.3
WT 50 µM Ca^{2+}[b]	7	−7 ± 1	14.6 ± 0.9	ND	ND	−54 ± 1	9.2 ± 0.9
D456C 50 µM Ca^{2+}[b]	6	37 ± 1	11.5 ± 0.4	ND	ND	4 ± 2	14.7 ± 0.7
D460C 50 µM Ca^{2+}[b]	4	26 ± 3	10.6 ± 0.3	ND	ND	6 ± 4	19 ± 1
D509C 50 µM Ca^{2+}[b]	6	25 ± 3	15.3 ± 0.7	ND	ND	6 ± 4	16.1 ± 0.3

n, number of measurements; V_{50}, half-maximal activation voltage; *s*, slope factor.

[a]Values reported for 8-s test depolarization steps as shown in Fig. 4.

[b]There are no pH 7 values listed because we only thoroughly tested pH 6 and 8 to see whether this shift was changed in low Ca^{2+}.

but we focused on V_{50} shift to measure pH sensitivity. These results demonstrate that the EAG-specific acidic residues are required for high pH sensitivity in Kv12.1 and imply that these charges could be the site of antagonism between Zn^{2+} and protons. The universal acidic residue D261 is required for high Zn^{2+} sensitivity but not for pH sensitivity. V_{50} values for pH 6 and 8 and pH-dependent V_{50} shifts are plotted in Fig. 8, and V_{50} and slope factor values for all WT and mutant channels examined in this study are presented in Table 1.

We also examined the pH sensitivity of the charge-preserving mutations D261E, E265D, and D314E (Fig. 6, B–D). D314E eliminated pH sensitivity, but E265D did not significantly change the magnitude of the pH 8 to 6 V_{50} shift compared with WT (see Fig. 8 B). The variable effect of charge-preserving mutations at the EAG-specific sites suggests a role for side chain size as well as charge in formation of a proton modulation site. The relative shift of the voltage activation curve recorded for E265D at pH 7 away from the pH 8 curve and toward the pH 6 curve could indicate a higher pK_a for this mutant (Fig. 6 C), but we did not investigate the possibility further. The D261E mutation caused a significant gain of function, increasing the total V_{50} shift from pH 8 to 6 to 79 ± 3 mV (Fig. 6 B). Although an acidic residue at this position (D1) is not required for pH sensitivity in Kv12.1, the residue appears to be close enough to influence the site for pH modulation. Assuming that site is formed in part by E265 (E5) and/or D314 (D6), this idea is consistent with previous observations that all three S2/S3 acidic residues lie in close enough proximity to influence divalent sensitivity (Zhang et al., 2009).

Contributions of S4 residue H328 to pH sensitivity in Kv12.1

We tested whether histidine H328 in the outer S4 of Kv12.1 also influences pH sensitivity of voltage activation because it contributes to Zn^{2+} block (Zhang et al., 2009) and the typical pK_a of histidine is ∼6.4. However, we reasoned that H328 should not be required for pH sensitivity because the residue is conserved only within the Elk family and thus could not explain pH sensitivity in Eag and Erg channels. We measured V_{50} shifts between pH 6, 7, and 8 to assess the pH sensitivity of various Kv12.1 H328 mutants. Modulation by pH was minimally affected by the neutralization mutation H328A (Fig. 7 B), confirming that protonation of H328 is not necessary for the Kv12.1 pH response. However, introduction of a positively charged arginine residue at this site (H328R) dramatically slows activation, depolarizes the voltage activation curve, and eliminates Zn^{2+} sensitivity (Zhang et al., 2009). H328R also significantly decreased pH sensitivity, indicating that positive charge at position 328 may eliminate the proton-binding site or electrostatically block access to it (Fig. 7 C). Consistent with the V_{50} shifts, external acidification had a much greater effect on the activation time course of the pH-sensitive mutant H328A than the pH-resistant mutant H328R (Fig. S1). The pH sensitivity of H328R could be restored by simultaneous neutralization of D261, the universal D1 aspartate in the S2 transmembrane domain (Fig. 7 D). The ability to bring pH sensitivity back in the H328R mutant background provides further proof that H328 is not necessary for pH-dependent modulation of Kv12.1. The large aromatic substitution H328W also reduced

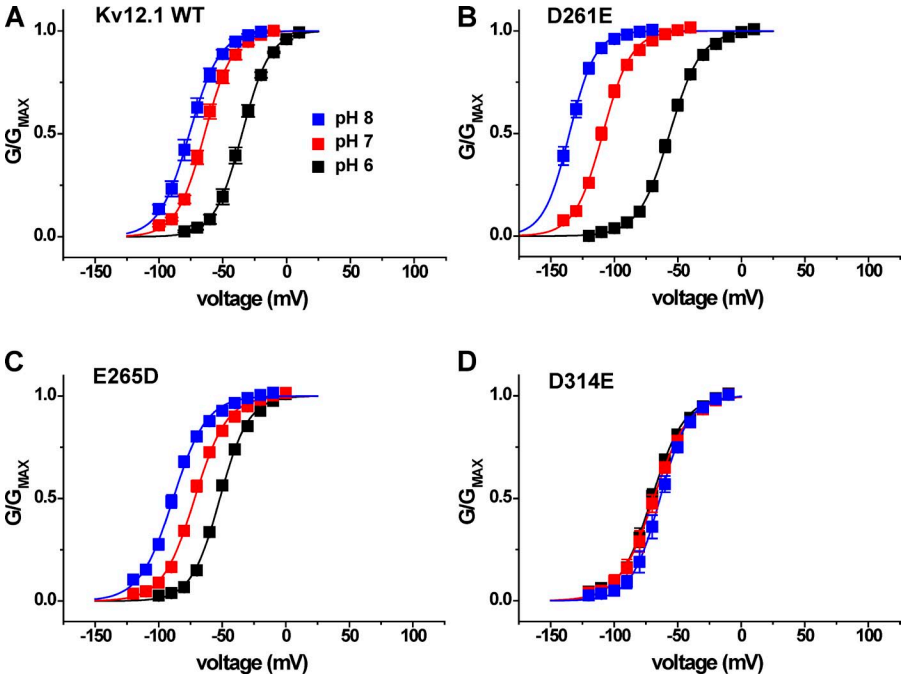

Figure 6. Effect of charge-preserving mutations at D1, E5, and D6 on the pH sensitivity of Kv12.1 channel. (A–D) Normalized GV relations are shown for WT Kv12.1, D261E (D1E), E265D (E5D), and D314E (D6E) at bath pH 6, 7, and 8. Conductance was determined from isochronal tail currents recorded at −40 mV after 8-s steps to the indicated voltages; values show mean ± SEM (n = 4–8), and curves show single Boltzmann distribution fits. Fit parameters (V_{50} and slope factor) are reported in Table 1.

pH sensitivity, suggesting that a steric disruption of the proton modulation site might also occur with substitutions at position 328 (Fig. 7 E). V_{50} shifts between pH 8 and 6 for these H328 mutants are summarized in Fig. 8. Similar results to those described above were found for the neutralization H328Q, the basic substitution H328K, and the aromatic substitution H328Y (Fig. S1). Insertion of negative charge (H328E) shifted the GV to the more hyperpolarized potentials but caused only a minor decrease in pH sensitivity (Fig. S1).

The mechanism of pH sensitivity is shared between Eag and Elk families

We next examined whether the same EAG-specific acidic residues confer high external pH sensitivity to Eag channels. External pH has previously been reported to slow activation and reduce Mg^{2+} sensitivity in rat Eag1 (Kv10.1; Terlau et al., 1996). We used the second mammalian Eag family orthologue, mouse Eag2 (Kv10.2), for these studies to verify whether external pH sensitivity is a common property of the gene family. Kv10.2 was more sensitive to changes in extracellular pH than the Elk channels in the absence of Mg^{2+}. Lowering external pH from 8 to 6 slowed the activation time course of Kv10.2 (Fig. 9, A and B) and caused a 71 ± 1–mV shift in the V_{50} of voltage-dependent activation (Figs. 9 C and 10 B). Neutralization of the EAG-specific acidic residues D5 and D6 (D255C and D304N) significantly decreased the shift of V_{50} induced by changing external pH from 8 to 6 to 22 ± 5 mV and 14 ± 1 mV, respectively (Fig. 9, E and F; and Fig. 10 B). These results demonstrate that the EAG-specific acidic residues in S2 and S3 are required for high sensitivity to external pH in both Eag and Elk channels. Neutralization of the universal D1 acidic residue D251 did not reduce the magnitude of the pH-dependent shift of V_{50} (Figs. 9 D and 10 B), a result which is also consistent with mutational analysis of Kv12.1. However, the charge-preserving D304E mutation at D6 in S3 (Fig. 9 G) did not reduce pH sensitivity as observed for Kv12.1, suggesting that aspartate is not strictly required at position 6 for pH sensitivity in all EAG superfamily channels. The D304E curves suggest a possible altered pK_a based on the relative positions of the GV curves at pH 6, 7, and 8, but we did not investigate this possibility further.

Voltage activation of Kv11.1 (hErg1) is highly pH sensitive in low external Ca^{2+}

We next examined the mechanism of pH sensitivity in the human Erg channel Kv11.1. Reported pH-dependent

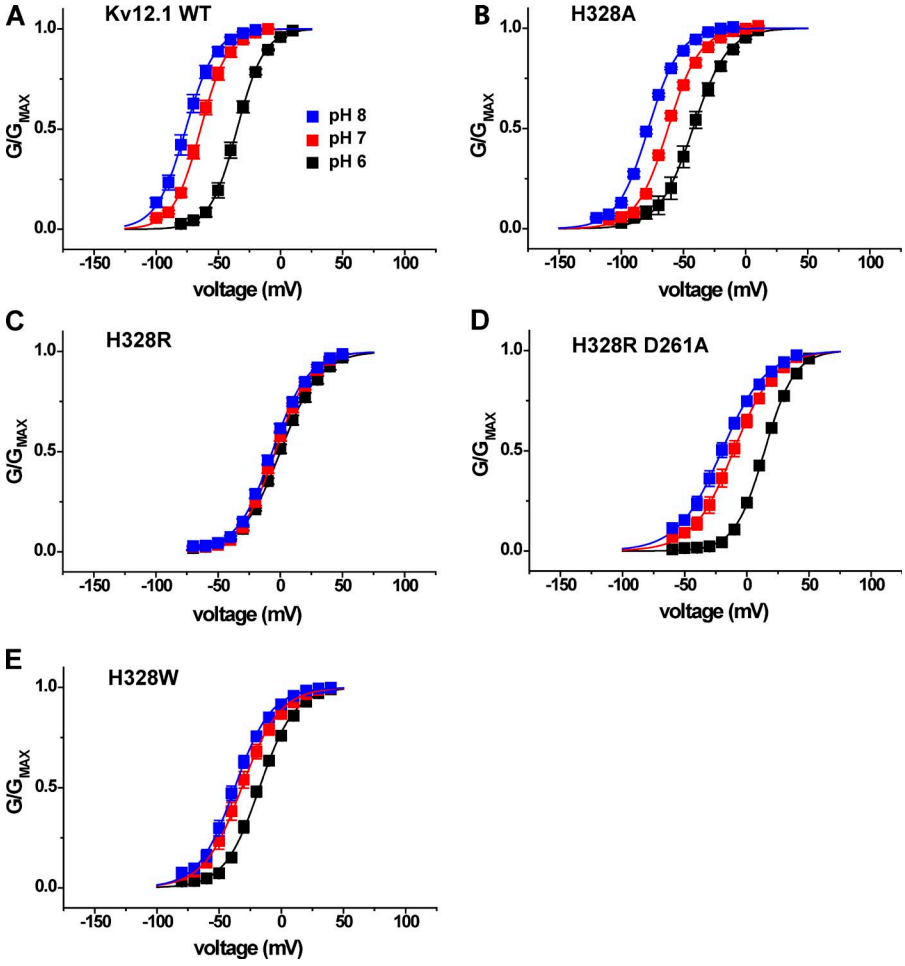

Figure 7. S4 histidine H328 is not required for sensitivity to extracellular pH in Kv12.1. (A–E) Normalized GV relations for Kv12.1 WT and S4 histidine mutants are shown at three bath pH values: pH 6, 7, and 8. Conductance was determined from isochronal tail currents recorded at −40 mV after 8-s steps to the indicated voltages. Data points show mean ± SEM, and curves represent single Boltzmann distribution fits; parameters and *n* are given in Table 1, and V_{50} shifts from pH 8 to 6 are reported in Fig. 8.

shifts in V_{50} for Kv11.1 are small in comparison with the large shifts we observed here for Kv10 and Kv12 channels (Anumonwo et al., 1999; Bérubé et al., 1999; Jiang et al., 1999; Jo et al., 1999; Terai et al., 2000). Furthermore, the pH-dependent inhibition of voltage activation in Kv11.1 is almost eliminated at 5 mM Ca^{2+} (Jo et al., 1999), and Ca^{2+} is known to block Kv11.1 at the divalent binding site (Johnson et al., 2001; Fernandez et al., 2005). We therefore examined the pH sensitivity of Kv11.1 at external Ca^{2+} concentrations ranging from 50 µM to 2 mM. GV curves for Kv11.1 are shown in Fig. 11 A at pH 8, 7, and 6 for 1 mM Ca^{2+} and at pH 8 and 6 for 50 µM Ca^{2+}. The shift in GV midpoint between pH 8 and 6 increased from 12.5 ± 0.5 mV in 1 mM Ca^{2+} to 47 ± 1 mV in 50 µM Ca^{2+} (Figs. 11 A and 12 B), indicating that protons and Ca^{2+} might compete for the same binding site, as observed for protons and Zn^{2+} in Kv12.1 and protons and Mg^{2+} in Kv10.1. Fig. 11 B shows a graph of the pH 8 to 6 V_{50} shifts recorded for Kv11.1 at various Ca^{2+} concentrations. The dose–response fit suggests that the pH-dependent shift we observe at 50 µM Ca^{2+} should be near maximal, and we therefore chose to test the effect of mutations on pH sensitivity at this Ca^{2+} concentration. Ca^{2+} has almost no effect on Kv12.1 and only a modest effect on Kv10.2 (not depicted), allowing high pH sensitivity to be observed in the 1 mM Ca^{2+} concentration we typically used in this study.

Conservation of the pH modulation mechanism in Kv11.1

Neutralization of the EAG-specific acidic residues D5 and D6 (D460C and D509C) significantly reduced the pH 8 to 6 V_{50} shift measured at 50 µM Ca^{2+} from 47 ± 1 mV to 21 ± 2 mV and 19 ± 3 mV, respectively (Fig. 11, C and D; and Fig. 12 B). We also observed a smaller but significant reduction in pH sensitivity for neutralization of the universal acidic residue D1 (D456C) to 33 ± 3 mV (Figs. 11 E and 12 B). These same acidic residue mutations have previously been reported to reduce Ca^{2+} block of Kv11.1 (Fernandez et al., 2005). Consistent with this result, we found that the pH 8 to 6 V_{50} shifts for D456C, D460C, and D509C were not significantly different at 50 µM and 1 mM Ca^{2+} (Figs. 11 F and 12 B). Therefore, at 1 mM Ca^{2+}, where the pH-dependent V_{50} shift in WT Kv11.1 is severely attenuated, the mutations D456C and D460C appear to increase pH sensitivity (Fig. 11 F). The loss of pH sensitivity in these mutants is only revealed at low Ca^{2+}.

DISCUSSION

We show here that EAG-specific acidic residues D/E5 and D6 in the S2 and S3 transmembrane domains of the voltage sensor confer high pH sensitivity to voltage gating in EAG superfamily channels. Neutralization of either D/E5 or D6 significantly reduces the V_{50} shift caused by external pH changes in representatives of the Eag, Elk, and Erg gene families. Thus all three subfamilies appear to share a common mechanism for pH-sensitive voltage activation. Both residues also contribute to the divalent cation-binding site of EAG superfamily channels (Silverman et al., 2000; Fernandez et al., 2005; Zhang et al., 2009). The major effect of both protons and divalent

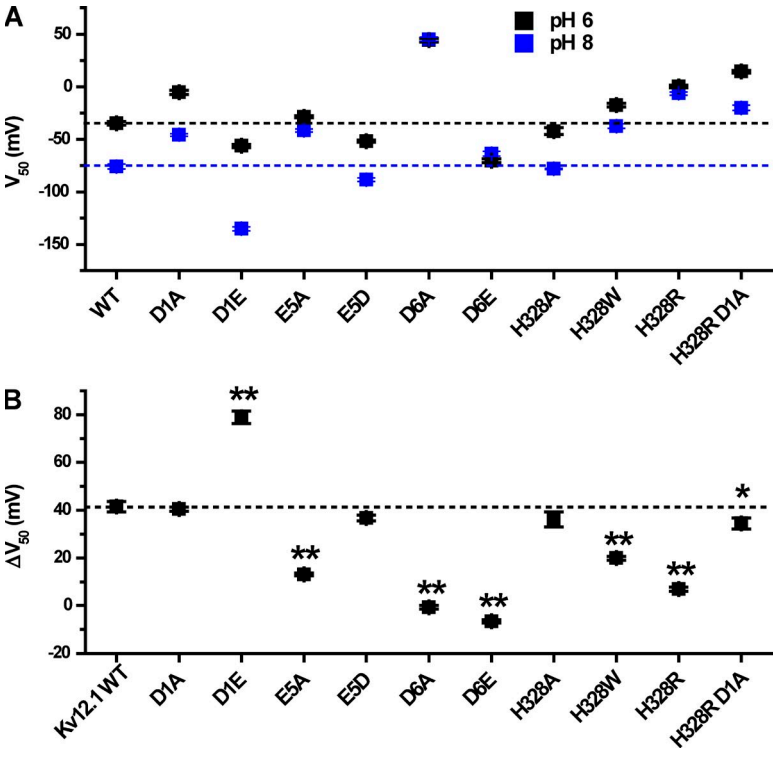

Figure 8. Comparison of V_{50} at pH 6 and 8 for Kv12.1 mutants. (A) V_{50} values are shown for pH 6 and 8 for WT and mutant Kv12.1 channels; values are taken from the single Boltzmann fits shown in Figs. 5–7. Dashed lines indicate the WT V_{50} values for pH 6 and 8. (B) Comparison of the pH 8 to 6 V_{50} shift for WT and mutant Kv12.1 channels. Shifts were calculated as a difference: $\Delta V_{50} = V_{50}$ (pH = 6) − V_{50} (pH = 8). The dashed line indicates the ΔV_{50} for Kv12.1 WT. Data points show mean ± SEM. Two-tailed nonequal variance Student's *t* test was used to judge significance of the differences in ΔV_{50}; asterisks indicate significant difference from WT: **, $P < 0.001$; and *, $P < 0.05$.

cations on voltage gating of EAG superfamily channels is to cause a large, depolarizing shift in the GV curve. These results are therefore consistent with the previous observation that protons and Mg^{2+} compete to inhibit voltage activation in Kv10.1 (Terlau et al., 1996), and our finding that protons and Zn^{2+} compete to inhibit Kv12.1. Furthermore, we found that Ca^{2+} greatly reduces the pH sensitivity of Kv11.1, or hErg1. Voltage activation in Kv11.1 is far more sensitive to pH than previously appreciated when measurements are made in low Ca^{2+}.

Although our results clearly demonstrate that EAG-specific acidic residues are required for highly pH-sensitive voltage activation in EAG superfamily channels, the exact identity of the proton-binding site is still not certain. The EAG-specific acidic residues themselves are attractive candidates for the binding site because they are the only outer voltage sensor residues conserved across the entire EAG superfamily that are both required for pH sensitivity and have the potential for proton titration across the pH range we tested. Furthermore, competition between protons and divalent cations suggests that the proton-binding site overlaps the divalent binding site, which includes these residues. Structural models supported by divalent binding experiments suggest that the EAG-specific acidic residues lie in close proximity to each other; therefore, it is possible that they could have physiologically relevant pK_a values instead of the typical low pK_a (<5) of isolated acidic side chains (Harris and Turner, 2002). Structural experiments of the acid-sensing cation channel ASIC1 strongly suggest that carboxyl–carboxylate interactions between neighboring acidic residues mediate its physiologically relevant pH sensitivity (Jasti et al., 2007). If a similar mechanism is at play in EAG superfamily channels, it could provide an explanation for why individual neutralizations within the EAG-specific acidic residue pair would greatly reduce pH

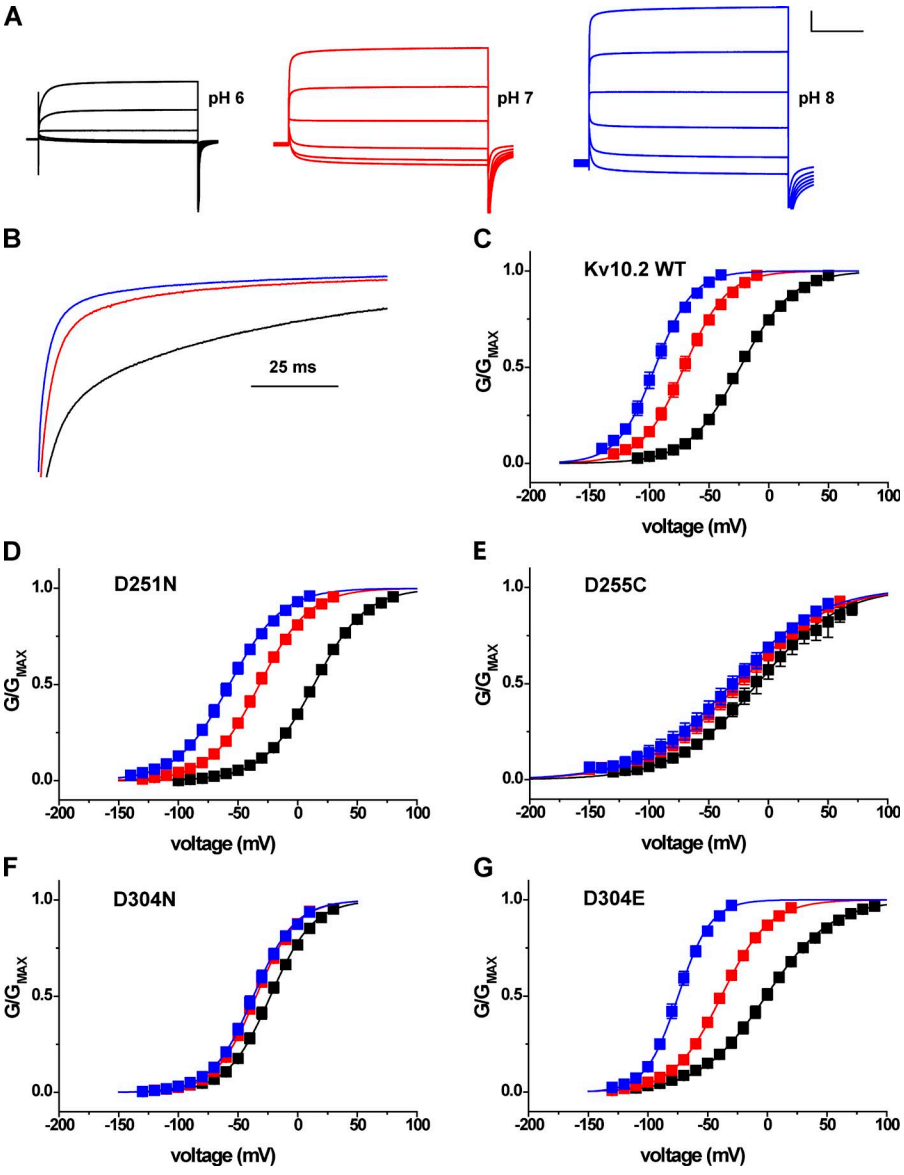

Figure 9. High sensitivity to extracellular pH in Kv10.2 is conferred by EAG-specific acidic residues in the voltage sensor. (A) Kv10.2 current traces elicited by 2-s depolarization steps from −80 to 20 mV in 20-mV increments in bath pH 6, 7, and 8. 50 mM bath K^+ was used to accentuate inward tail currents at the −100-mV holding potential. Scale bar: 1 µA, 500 ms. (B) Current traces recorded at 20 mV were normalized and superimposed to illustrate the effect of bath pH on activation time course. pH is encoded by color as in A. (C) Normalized GV relations for Kv10.2 obtained from isochronal tail current measurements at −100 mV in 50 mM K^+ after 2-s steps to the indicated voltages in pH 6 (black), 7 (red), and 8 (blue). (D–G) Similar GV curves obtained for Kv10.2 voltage sensor acidic residue mutants D251N (D1N), D255C (D5C) D304N (D6N), and D304E (D6E). Data points in C–G show mean ± SEM (n = 4–10), and curves show single Boltzmann distribution fits; V_{50}, slope factors, and ΔV_{50} (pH 8 to 6) are reported in Table 1 and Fig. 10.

sensitivity. The remaining acidic residue could potentially still bind protons, but with a reduced pK_a that would limit the V_{50} shift observed above pH 6. This possibility is not easily testable because of severe block of ion conduction at pH values below those we investigated.

The ability of mutations at D1 (D261) and H328 in Kv12.1 to enhance or attenuate pH sensitivity, respectively, supports the idea that the proton modulation site is at least close to the EAG-specific charges. A previous study suggests that these residues also participate in divalent cation coordination and thus must lie in close proximity to the EAG-specific charges in the closed channel (Zhang et al., 2009). We speculate that the mutations at these sites could alter pH sensitivity through electrostatic or steric interaction with the proton-binding site or by altering voltage sensor conformation. For instance, the depolarized GV curve and slow activation of H328R could reflect the formation of an additional salt bridge (in the closed voltage sensor) that is broken by simultaneous neutralization of D261. However, neither of these residues appears to participate in the key proton-binding event because neither is required for pH-dependent GV shifts.

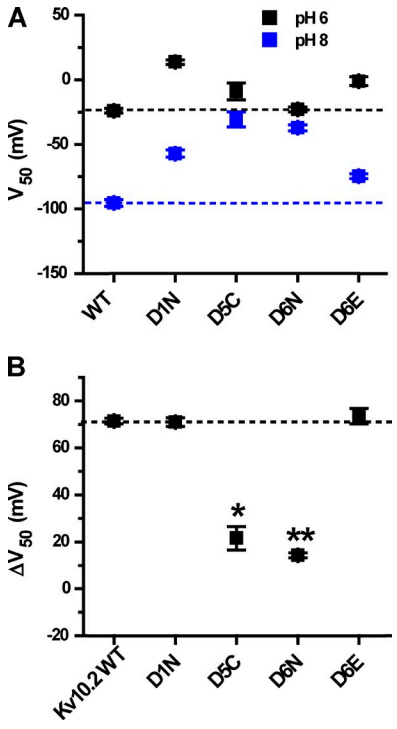

Figure 10. Shifts in V_{50} caused by the change of external pH from 8 to 6 for Kv10.2 mutants. (A) V_{50} values are shown for pH 6 and 8 for mouse Kv10.2 channel and its mutants; dashed lines are extended across the figure to indicate the WT values. V_{50} values were obtained from Boltzmann fits shown in Fig. 9 (C–G). (B) ΔV_{50} (pH 8 to 6) plots for Kv10.2 WT and S2/S3 acidic residue mutants. Significance was tested with a two-tailed nonequal variance Student's *t* test; asterisks indicate significant difference with respect to WT: **, $P < 0.001$; and *, $P < 0.005$. The dashed line indicates the value of ΔV_{50} (pH 8 to 6) for WT Kv10.2.

Mechanistic studies of divalent cation block and the crystal structure of the voltage sensor of a Shaker chimaera provide a speculative model of how direct protonation of the EAG-specific charges could inhibit voltage-dependent activation. Silverman et al. (2003) proposed that basic S4 gating charges sequentially move through the aqueous cleft (in which the EAG-specific acidic residues D/E5 and D6 reside) during activation to form salt bridges with the universally conserved acidic residue at position D1. Divalent cations occupying the cleft and coordinated in part by D/E5 and D6 block the forward movement of S4 charges in this model. Support for the model comes from observations that Cd^{2+} depolarizes gating charge movement in Kv11.1 (Abbruzzese et al., 2010) and that Mg^{2+} modulates structural movements that precede observable gating charge movement in *Drosophila* Eag (Bannister et al., 2005). Furthermore, salt bridge pairing of an S4 basic charge with E1 in S2 occurs in the crystal structure of the activated voltage sensor of a chimeric Shaker channel (Long et al., 2007). The role of the EAG-specific acidic residues in voltage activation has not been conclusively defined, but it is tempting to speculate that the additional negative charges could somehow facilitate movement of basic S4 gating charges. Direct protonation or mutational neutralization of these acidic residues would reduce net negative charge and could therefore inhibit voltage sensor activation as observed here.

Although our results are consistent with a model of direct protonation of the EAG-specific charge pair as the mechanism of pH sensitivity, they do not rule out an alternative hypothesis. The gating models and crystal structure described above make it clear that mutation of charged voltage sensor residues could have significant effects on voltage sensor conformation. Therefore, it remains possible that the EAG-specific residues are simply necessary to hold the voltage sensor in a pH-sensitive conformation. Neutralization of the charges could then lead to conformational changes that allosterically disrupt a separate proton-binding site. Alternatively, conformational changes in the absence of the EAG-specific acidic residues could simply block access to the proton modulation site.

The finding that the EAG-specific acidic residues of the voltage sensor are required for pH-dependent modulation predicts that high pH sensitivity across the physiological range should be a general property of Eag superfamily channels. Previous studies indicated that rat Kv10.1, human Kv11.1, and rat Kv12.1 are inhibited by extracellular acidosis (Terlau et al., 1996; Shi et al., 1998). We extend those studies here to show that Kv10.2, Kv12.2, and Kv12.3 are similarly modulated by external pH. Thus high pH sensitivity has now been observed for six of eight mammalian EAG superfamily orthologues, including all members of the Eag and Elk gene families. The Erg family channels Kv11.2 and Kv11.3 have

not yet been examined for pH sensitivity, but they also have the EAG-specific acidic residues.

The physiological relevance of pH-sensitive voltage gating in EAG superfamily channels has yet to be determined. However, the pH-dependent GV shifts we see here predict that modest changes in pH around the physiological range could have significant effects on current at the subthreshold potentials, where EAG superfamily channels can demonstrably affect neuronal excitability (Zhang et al., 2010). Even small pH changes around the physiological range affect holding current in Kv12-expressing HEK293 cells, highlighting the potential of these channels to contribute to pH-sensitive K^+ currents in vivo. We therefore suggest that EAG superfamily channels should be treated as candidates of interest for pH-sensitive K^+ currents of unknown molecular identity. Elk channels have perhaps the highest potential for significant pH modulation in vivo because they show high pH sensitivity at typical extracellular Mg^{2+} and Ca^{2+} concentrations. We tested Kv12.1 and Kv12.2 here in 1 mM Mg^{2+} and 1 mM Ca^{2+}. Eag channel pH sensitivity is attenuated by Mg^{2+} but remains significant even up to 1 mM (Terlau et al., 1996) and therefore is still likely to exist in vivo. The pH sensitivity of Kv11.1 voltage gating is largely masked at physiological extracellular Ca^{2+} concentrations, so its importance in vivo is less clear. However, acidification independently reduces Kv11.1 conductance, and a potential role for the channel in modulating the effects of myocardial ischemic acidosis and the associated arrhythmias has been hypothesized (Van Slyke et al., 2012).

We suggest that Eag and Elk channels could contribute to a neuronal pH-sensitive K^+ current characterized as either a voltage-dependent or leak conductance. Eag and Elk family potassium channels are activated at resting voltages, and their voltage dependence is relatively shallow and could easily be missed when examining a limited voltage range. Therefore, it is possible that potassium currents flowing through these channels could in some cases be interpreted as leak currents. This could be particularly relevant to the respiratory system where an unidentified pH-sensitive leak K^+ current is thought to underlie the mechanism by which neurons in the retrotrapezoid nucleus regulate breathing in response to changes in tissue pH (Mulkey et al., 2004, 2007). Genetic and pharmacological studies will be needed to reveal

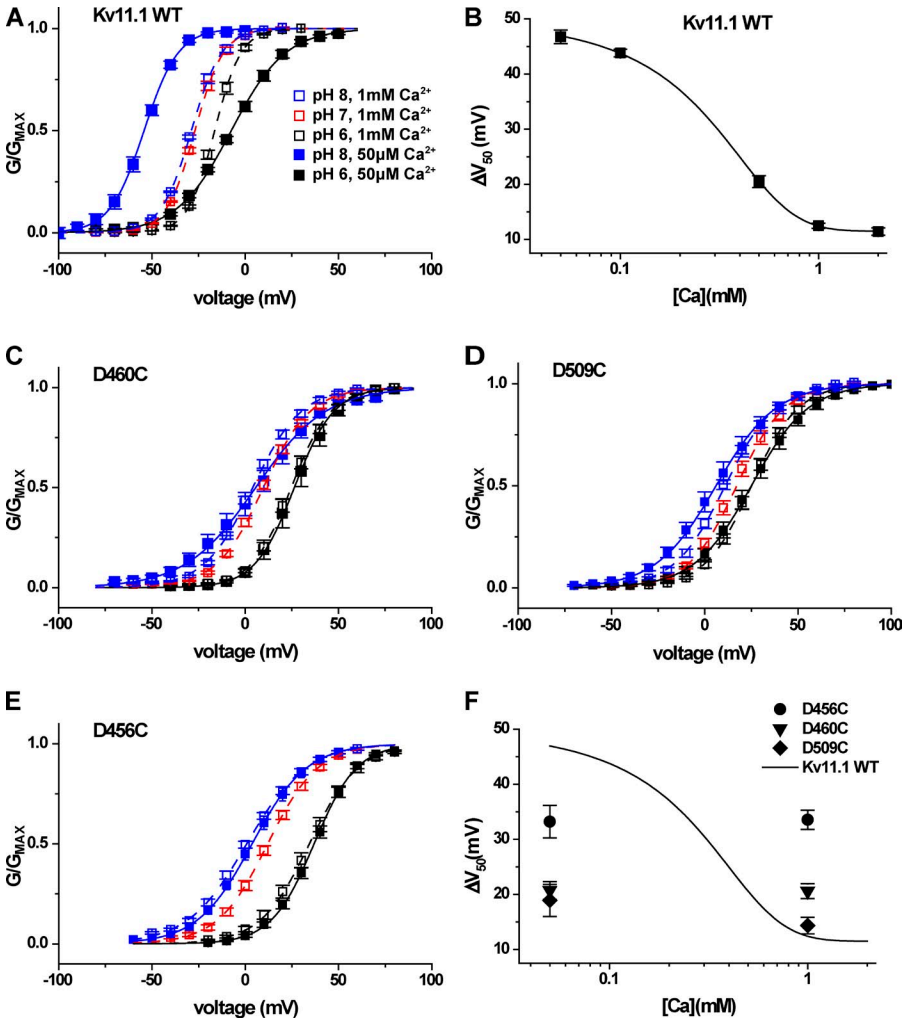

Figure 11. High pH sensitivity of Kv11.1 is revealed at low Ca^{2+} and depends on the EAG-specific acidic charges. (A) Normalized GV relations for Kv11.1 are shown for pH 6, 7, and 8 at 1 mM Ca^{2+} and for pH 6 and 8 at 50 µM Ca^{2+}. Conductance values were determined from isochronal tail currents recorded at −40 mV after 4-s steps to the indicated voltages from a −100-mV holding potential. Data points show mean ± SEM (n = 4–10), and curves show Boltzmann fits; V_{50}, slope factors, and ΔV_{50} (pH 8 to 6) are reported in Table 1 and Fig. 12. (B) ΔV_{50} (pH 8 to 6) for WT Kv11.1 is plotted as a function of Ca^{2+} concentration and fitted with a four-parameter dose–response curve. Log_{10} scale is applied to the Ca^{2+} concentration, and data points show mean ± SEM. (C–E) Normalized GV relationships for the EAG-specific charge mutants D460C (D5C) and D509C (D6C) and the universal acidic charge mutant D456C (D1C) are shown for pH 6, 7, and 8 at 1 mM Ca^{2+} and pH 6 and 8 at 50 µM Ca^{2+}. Conditions are coded by shading and color as in A. Single Boltzmann fit parameters and ΔV_{50} (pH 8 to 6) are reported in Table 1 and Fig. 12, respectively. (F) ΔV_{50} (pH 8 to 6) for Kv11.1 acidic neutralization mutants at 50 µM and 1 mM Ca^{2+} are presented in comparison with the Kv11.1 WT fit curve from B.

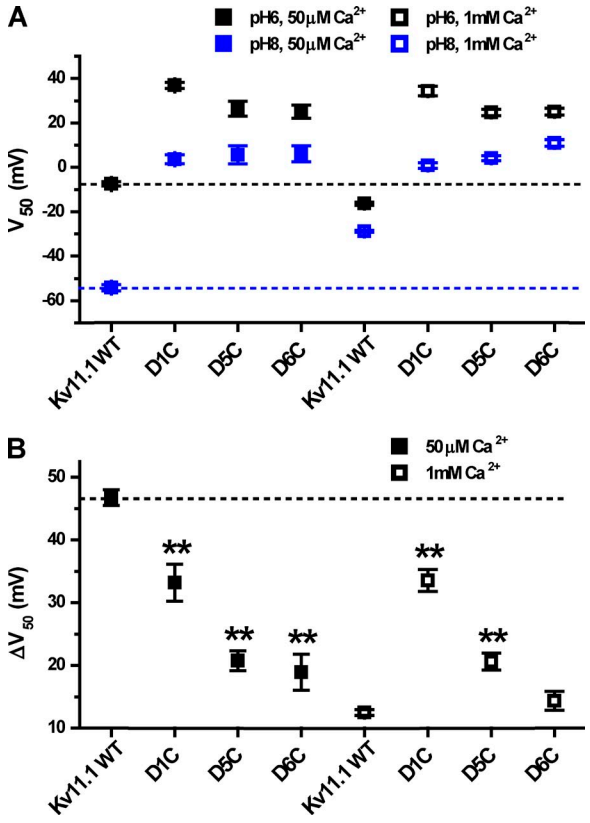

Figure 12. Analysis of V_{50} at external pH 8 and 6 for Kv11.1 mutants. (A) V_{50} values are shown for pH 6 and 8 for WT Kv11.1 and Kv11.1 acidic charge-neutralization mutants (dashed lines indicate WT values). The values of V_{50} were obtained from Boltzmann fits shown in Fig. 11 (A and C–E). (B) ΔV_{50} (pH 8 to 6) plots for Kv11.1 WT and the S2/S3 acidic charge-neutralization mutants at 50 µM Ca^{2+} and 1 mM Ca^{2+}. The dashed line indicates the ΔV_{50} obtained for WT Kv11.1. Asterisks indicate significant difference with respect to WT: **, $P < 0.001$; two-tailed nonequal variance Student's *t* test.

whether the pH sensitivity observed for EAG superfamily channels in vitro contributes to neurophysiology in vivo.

This work was supported by National Institutes of Health grants R01 NS069842 (to T. Jegla), R01 HL108609 (to D.A. Bayliss), and R01 HL104101 (to D.K. Mulkey) and the Penn State Department of Biology.

Sharona E. Gordon served as editor.

Submitted: 19 November 2012
Accepted: 30 April 2013

REFERENCES

Abbruzzese, J., F.B. Sachse, M. Tristani-Firouzi, and M.C. Sanguinetti. 2010. Modification of hERG1 channel gating by Cd^{2+}. *J. Gen. Physiol.* 136:203–224. http://dx.doi.org/10.1085/jgp.201010450

Agarwal, J.R., F. Griesinger, W. Stühmer, and L.A. Pardo. 2010. The potassium channel Ether à go-go is a novel prognostic factor with functional relevance in acute myeloid leukemia. *Mol. Cancer.* 9:18. http://dx.doi.org/10.1186/1476-4598-9-18

Anumonwo, J.M., J. Horta, M. Delmar, S.M. Taffet, and J. Jalife. 1999. Proton and zinc effects on HERG currents. *Biophys. J.* 77: 282–298. http://dx.doi.org/10.1016/S0006-3495(99)76889-X

Bannister, J.P., B. Chanda, F. Bezanilla, and D.M. Papazian. 2005. Optical detection of rate-determining ion-modulated conformational changes of the ether-à-go-go K+ channel voltage sensor. *Proc. Natl. Acad. Sci. USA.* 102:18718–18723. http://dx.doi.org/10.1073/pnas.0505766102

Berg, A.P., E.M. Talley, J.P. Manger, and D.A. Bayliss. 2004. Motoneurons express heteromeric TWIK-related acid-sensitive K+ (TASK) channels containing TASK-1 (KCNK3) and TASK-3 (KCNK9) subunits. *J. Neurosci.* 24:6693–6702. http://dx.doi.org/10.1523/JNEUROSCI.1408-04.2004

Bérubé, J., M. Chahine, and P. Daleau. 1999. Modulation of HERG potassium channel properties by external pH. *Pflugers Arch.* 438:419–422. http://dx.doi.org/10.1007/s004240050930

Cho, S.Y., E.A. Beckett, S.A. Baker, I. Han, K.J. Park, K. Monaghan, S.M. Ward, K.M. Sanders, and S.D. Koh. 2005. A pH-sensitive potassium conductance (TASK) and its function in the murine gastrointestinal tract. *J. Physiol.* 565:243–259. http://dx.doi.org/10.1113/jphysiol.2005.084574

Duprat, F., F. Lesage, M. Fink, R. Reyes, C. Heurteaux, and M. Lazdunski. 1997. TASK, a human background K+ channel to sense external pH variations near physiological pH. *EMBO J.* 16:5464–5471. http://dx.doi.org/10.1093/emboj/16.17.5464

Fernandez, D., A. Ghanta, K.I. Kinard, and M.C. Sanguinetti. 2005. Molecular mapping of a site for Cd2+-induced modification of human ether-à-go-go-related gene (hERG) channel activation. *J. Physiol.* 567:737–755. http://dx.doi.org/10.1113/jphysiol.2005.089094

Ganetzky, B., and C.F. Wu. 1983. Neurogenetic analysis of potassium currents in *Drosophila*: synergistic effects on neuromuscular transmission in double mutants. *J. Neurogenet.* 1:17–28. http://dx.doi.org/10.3109/01677068309107069

Gestreau, C., D. Heitzmann, J. Thomas, V. Dubreuil, S. Bandulik, M. Reichold, S. Bendahhou, P. Pierson, C. Sterner, J. Peyronnet-Roux, et al. 2010. Task2 potassium channels set central respiratory CO2 and O2 sensitivity. *Proc. Natl. Acad. Sci. USA.* 107:2325–2330. http://dx.doi.org/10.1073/pnas.0910059107

González, J.A., L.T. Jensen, S.E. Doyle, M. Miranda-Anaya, M. Menaker, L. Fugger, D.A. Bayliss, and D. Burdakov. 2009. Deletion of TASK1 and TASK3 channels disrupts intrinsic excitability but does not abolish glucose or pH responses of orexin/hypocretin neurons. *Eur. J. Neurosci.* 30:57–64. http://dx.doi.org/10.1111/j.1460-9568.2009.06789.x

Guyon, A., M.P. Tardy, C. Rovère, J.L. Nahon, J. Barhanin, and F. Lesage. 2009. Glucose inhibition persists in hypothalamic neurons lacking tandem-pore K+ channels. *J. Neurosci.* 29:2528–2533. http://dx.doi.org/10.1523/JNEUROSCI.5764-08.2009

Hardman, R.M., and I.D. Forsythe. 2009. Ether-à-go-go-related gene K+ channels contribute to threshold excitability of mouse auditory brainstem neurons. *J. Physiol.* 587:2487–2497. http://dx.doi.org/10.1113/jphysiol.2009.170548

Harris, T.K., and G.J. Turner. 2002. Structural basis of perturbed pKa values of catalytic groups in enzyme active sites. *IUBMB Life.* 53:85–98. http://dx.doi.org/10.1080/15216540211468

Hemmerlein, B., R.M. Weseloh, F. Mello de Queiroz, H. Knötgen, A. Sánchez, M.E. Rubio, S. Martin, T. Schliephacke, M. Jenke, Heinz-Joachim-Radzun, et al. 2006. Overexpression of Eag1 potassium channels in clinical tumours. *Mol. Cancer.* 5:41. http://dx.doi.org/10.1186/1476-4598-5-41

Jasti, J., H. Furukawa, E.B. Gonzales, and E. Gouaux. 2007. Structure of acid-sensing ion channel 1 at 1.9 Å resolution and low pH. *Nature.* 449:316–323. http://dx.doi.org/10.1038/nature06163

Jegla, T., and L. Salkoff. 1997. A novel subunit for shal K+ channels radically alters activation and inactivation. *J. Neurosci.* 17:32–44.

Ji, H., K.R. Tucker, I. Putzier, M.A. Huertas, J.P. Horn, C.C. Canavier, E.S. Levitan, and P.D. Shepard. 2012. Functional characterization of ether-à-go-go-related gene potassium channels in midbrain dopamine neurons – implications for a role in depolarization

block. *Eur. J. Neurosci.* 36:2906–2916. http://dx.doi.org/10.1111/j.1460-9568.2012.08190.x

Jiang, M., W. Dun, and G.N. Tseng. 1999. Mechanism for the effects of extracellular acidification on HERG-channel function. *Am. J. Physiol.* 277:H1283–H1292.

Jo, S.H., J.B. Youm, I. Kim, C.O. Lee, Y.E. Earm, and W.K. Ho. 1999. Blockade of HERG channels expressed in *Xenopus* oocytes by external H+. *Pflugers Arch.* 438:23–29. http://dx.doi.org/10.1007/s004240050875

Johnson, J.P. Jr., J.R. Balser, and P.B. Bennett. 2001. A novel extracellular calcium sensing mechanism in voltage-gated potassium ion channels. *J. Neurosci.* 21:4143–4153.

Kim, Y., H. Bang, and D. Kim. 2000. TASK-3, a new member of the tandem pore K(+) channel family. *J. Biol. Chem.* 275:9340–9347. http://dx.doi.org/10.1074/jbc.275.13.9340

Lin, W., C.A. Burks, D.R. Hansen, S.C. Kinnamon, and T.A. Gilbertson. 2004. Taste receptor cells express pH-sensitive leak K+ channels. *J. Neurophysiol.* 92:2909–2919. http://dx.doi.org/10.1152/jn.01198.2003

Long, S.B., X. Tao, E.B. Campbell, and R. MacKinnon. 2007. Atomic structure of a voltage-dependent K+ channel in a lipid membrane-like environment. *Nature.* 450:376–382. http://dx.doi.org/10.1038/nature06265

Mulkey, D.K., R.L. Stornetta, M.C. Weston, J.R. Simmons, A. Parker, D.A. Bayliss, and P.G. Guyenet. 2004. Respiratory control by ventral surface chemoreceptor neurons in rats. *Nat. Neurosci.* 7:1360–1369. http://dx.doi.org/10.1038/nn1357

Mulkey, D.K., E.M. Talley, R.L. Stornetta, A.R. Siegel, G.H. West, X. Chen, N. Sen, A.M. Mistry, P.G. Guyenet, and D.A. Bayliss. 2007. TASK channels determine pH sensitivity in select respiratory neurons but do not contribute to central respiratory chemosensitivity. *J. Neurosci.* 27:14049–14058. http://dx.doi.org/10.1523/JNEUROSCI.4254-07.2007

Putzke, C., K. Wemhöner, F.B. Sachse, S. Rinné, G. Schlichthörl, X.T. Li, L. Jaé, I. Eckhardt, E. Wischmeyer, H. Wulf, et al. 2007. The acid-sensitive potassium channel TASK-1 in rat cardiac muscle. *Cardiovasc. Res.* 75:59–68. http://dx.doi.org/10.1016/j.cardiores.2007.02.025

Rajan, S., E. Wischmeyer, G. Xin Liu, R. Preisig-Müller, J. Daut, A. Karschin, and C. Derst. 2000. TASK-3, a novel tandem pore domain acid-sensitive K+ channel. An extracellular histiding as pH sensor. *J. Biol. Chem.* 275:16650–16657. http://dx.doi.org/10.1074/jbc.M000030200

Reyes, R., F. Duprat, F. Lesage, M. Fink, M. Salinas, N. Farman, and M. Lazdunski. 1998. Cloning and expression of a novel pH-sensitive two pore domain K+ channel from human kidney. *J. Biol. Chem.* 273:30863–30869. http://dx.doi.org/10.1074/jbc.273.47.30863

Sanguinetti, M.C., and M. Tristani-Firouzi. 2006. hERG potassium channels and cardiac arrhythmia. *Nature.* 440:463–469. http://dx.doi.org/10.1038/nature04710

Schönherr, R., G. Gessner, K. Löber, and S.H. Heinemann. 2002. Functional distinction of human EAG1 and EAG2 potassium channels. *FEBS Lett.* 514:204–208. http://dx.doi.org/10.1016/S0014-5793(02)02365-7

Shi, W., H.S. Wang, Z. Pan, R.S. Wymore, I.S. Cohen, D. McKinnon, and J.E. Dixon. 1998. Cloning of a mammalian elk potassium channel gene and EAG mRNA distribution in rat sympathetic ganglia. *J. Physiol.* 511:675–682. http://dx.doi.org/10.1111/j.1469-7793.1998.675bg.x

Silverman, W.R., C.Y. Tang, A.F. Mock, K.B. Huh, and D.M. Papazian. 2000. Mg^{2+} modulates voltage-dependent activation in ether-à-go-go potassium channels by binding between transmembrane segments S2 and S3. *J. Gen. Physiol.* 116:663–678. http://dx.doi.org/10.1085/jgp.116.5.663

Silverman, W.R., B. Roux, and D.M. Papazian. 2003. Structural basis of two-stage voltage-dependent activation in K+ channels. *Proc. Natl. Acad. Sci. USA.* 100:2935–2940. http://dx.doi.org/10.1073/pnas.0636603100

Silverman, W.R., J.P. Bannister, and D.M. Papazian. 2004. Binding site in eag voltage sensor accommodates a variety of ions and is accessible in closed channel. *Biophys. J.* 87:3110–3121. http://dx.doi.org/10.1529/biophysj.104.044602

Srinivasan, S., K. Lance, and R.B. Levine. 2012. Contribution of EAG to excitability and potassium currents in *Drosophila* larval motoneurons. *J. Neurophysiol.* 107:2660–2671. http://dx.doi.org/10.1152/jn.00201.2011

Tang, C.Y., F. Bezanilla, and D.M. Papazian. 2000. Extracellular Mg^{2+} modulates slow gating transitions and the opening of *Drosophila* ether-à-Go-Go potassium channels. *J. Gen. Physiol.* 115:319–338. http://dx.doi.org/10.1085/jgp.115.3.319

Terai, T., T. Furukawa, Y. Katayama, and M. Hiraoka. 2000. Effects of external acidosis on HERG current expressed in *Xenopus* oocytes. *J. Mol. Cell. Cardiol.* 32:11–21. http://dx.doi.org/10.1006/jmcc.1999.1048

Terlau, H., J. Ludwig, R. Steffan, O. Pongs, W. Stühmer, and S.H. Heinemann. 1996. Extracellular Mg2+ regulates activation of rat eag potassium channel. *Pflugers Arch.* 432:301–312. http://dx.doi.org/10.1007/s004240050137

Ufartes, R., T. Schneider, L.S. Mortensen, C. de Juan Romero, K. Hentrich, H. Knoetgen, V. Beilinson, W. Moebius, V. Tarabykin, F. Alves, et al. 2013. Behavioural and functional characterization of Kv10.1 (Eag1) knockout mice. *Hum. Mol. Genet.* http://dx.doi.org/10.1093/hmg/ddt076

Van Slyke, A.C., Y.M. Cheng, P. Mafi, C.R. Allard, C.M. Hull, Y.P. Shi, and T.W. Claydon. 2012. Proton block of the pore underlies the inhibition of hERG cardiac K+ channels during acidosis. *Am. J. Physiol. Cell Physiol.* 302:C1797–C1806. http://dx.doi.org/10.1152/ajpcell.00324.2011

Wimmers, S., I. Wulfsen, C.K. Bauer, and J.R. Schwarz. 2001. Erg1, erg2 and erg3 K channel subunits are able to form heteromultimers. *Pflugers Arch.* 441:450–455. http://dx.doi.org/10.1007/s004240000467

Wu, C.F., B. Ganetzky, F.N. Haugland, and A.X. Liu. 1983. Potassium currents in *Drosophila*: different components affected by mutations of two genes. *Science.* 220:1076–1078. http://dx.doi.org/10.1126/science.6302847

Yamanaka, A., C.T. Beuckmann, J.T. Willie, J. Hara, N. Tsujino, M. Mieda, M. Tominaga, Ki. Yagami, F. Sugiyama, K. Goto, et al. 2003. Hypothalamic orexin neurons regulate arousal according to energy balance in mice. *Neuron.* 38:701–713. http://dx.doi.org/10.1016/S0896-6273(03)00331-3

Yu, F.H., and W.A. Catterall. 2004. The VGL-chanome: a protein superfamily specialized for electrical signaling and ionic homeostasis. *Sci. STKE.* 2004:re15.

Zhang, X., B. Bursulaya, C.C. Lee, B. Chen, K. Pivaroff, and T. Jegla. 2009. Divalent cations slow activation of EAG family K+ channels through direct binding to S4. *Biophys. J.* 97:110–120. http://dx.doi.org/10.1016/j.bpj.2009.04.032

Zhang, X., F. Bertaso, J.W. Yoo, K. Baumgärtel, S.M. Clancy, V. Lee, C. Cienfuegos, C. Wilmot, J. Avis, T. Hunyh, et al. 2010. Deletion of the potassium channel Kv12.2 causes hippocampal hyperexcitability and epilepsy. *Nat. Neurosci.* 13:1056–1058. http://dx.doi.org/10.1038/nn.2610

Zhou, Q., and G.C. Bett. 2010. Regulation of the voltage-insensitive step of HERG activation by extracellular pH. *Am. J. Physiol. Heart Circ. Physiol.* 298:H1710–H1718. http://dx.doi.org/10.1152/ajpheart.01246.2009

Zou, A., Z. Lin, M. Humble, C.D. Creech, P.K. Wagoner, D. Krafte, T.J. Jegla, and A.D. Wickenden. 2003. Distribution and functional properties of human KCNH8 (Elk1) potassium channels. *Am. J. Physiol. Cell Physiol.* 285:C1356–C1366.